The International Journal of Advanced Manufacturing Technology (2019) 105:2771–2784
https://doi.org/10.1007/s00170-019-04461-z

ORIGINAL ARTICLE

Ductility-oriented high-speed grinding of silicon carbide and process design for quality and damage control with higher efficiency

Chongjun Wu[1] · Weicheng Guo[1] · Zhouping Wu[2] · Qingxia Wang[1] · Beizhi Li[1]

Received: 21 May 2019 / Accepted: 20 September 2019 / Published online: 8 November 2019

Abstract

Grinding of brittle materials is always a removal process of coexisting ductile and brittle removal modes. Ductility-oriented grinding has been regarded as a precision machining pursuit for grinding quality and efficiency. This paper is devoted to investigating ductility-oriented grinding mechanism and process design for quality promotion with a higher efficiency in high-speed grinding of silicon carbide ceramics. The Rayleigh chip thickness model and critical chip thickness model are given to quantitatively calculate the ductile removal proportion. Moreover, the grinding forces and specific removal energy are discussed to reflect the high-speed grinding removal mode. The results show that the increase of wheel speed or decrease of maximum chip thickness could enhance the percentage to a more ductile-oriented removal mode, which will cause a smaller surface roughness with fewer fracture cracks and more plastic removal stripes. Finally, the grinding process conditions for surface roughness below 0.2 μm and ductile removal area higher than 50% are suggested to obtain better surface quality at higher ductile removal and material removal rates.

Keywords Ductile grinding · Silicon carbide · Process design · Grinding damages · Grinding quality

1 Introduction

As a typical brittle material, silicon carbide (SiC) ceramics are commonly used in aerospace, medical, and semiconductor engineering applications for its superior performance of wear, heat, and chemical resistance and fantastic hardness [1–3]. However, the precision machining of ceramics is generally affected by inevitable crack generation, which will deteriorate the machining quality and efficiency. Grinding with diamond abrasive wheel, especially in the high-speed grinding (HSG) process, is widely used to diminish machining damages and improve surface finish for ceramics machining [4–7]. Therefore, the understanding of grinding material removal mechanism is crucial for better grinding quality with good efficiency [8].

✉ Qingxia Wang
wqxia@dhu.edu.cn

[1] College of Mechanical Engineering, Donghua University, Shanghai 201620, China

[2] Shanghai Spaceflight Manufacture (Group) Co., Ltd., Shanghai 200245, China

High-speed grinding is generally characterized by an elevated wheel speed above 60 m/s. In the HSG process, the abrasive grit will interact with the workpiece material at a higher frequency than conventional speed, which will substantially reduce the grinding chip thickness and thus reduce grinding forces and wheel wear [9]. In the past, the HSG process has been used as a finishing process which is beneficial to the transition of brittle grinding to ductile grinding for brittle materials. This is the effect of a high strain rate brought by high-grinding wheel speed, which may cause the material to produce a high strain rate of up to 10^{-5}~10^{-7}/s [10–11]. It is believed that the materials will get toughened at a high strain rate, and thus the ability to prevent crack generation will get enhanced [10]. That is how the HSG process helps control grinding damages and facilitates the ductile grinding process.

In grinding ceramics, the material is generally removed by a coexisting mechanism of ductile and brittle modes. In ductile grinding, it is believed that the material could be removed mainly by plastic deformation when the chip thickness is less than critical chip thickness [12–13]. This chip thickness model was determined by a critical energy model proposed by Bifano et al. [13], which is independent of process parameters, only connected with the material properties. Later on, the critical chip thickness model for ductile grinding was remodeled

by considering the effect of process parameters [14]. Therefore, the determination of ductile grinding cannot be merely obtained by full ductile grinding or brittle grinding, it is a combined process of the two removal modes. The method to quantitatively calculate the percentage of ductile removal could be more efficient and applicable for quality control.

In order to model the grinding kinematics, the grinding chip thickness for a single grit is generally assumed as a statistical distribution model [15], which could well match the stochastic feature of the grit–workpiece interaction. Gaussian [16–17] and Rayleigh [18–19] distributions are commonly used distributions. The Rayleigh chip thickness model was validated experimentally by measuring the grinding chip size for metals [18], also validated through the determination of surface topography in ceramics [20]. Therefore, the determination of ductile-oriented grinding proportion could be calculated through the chip thickness of all the active grits. This could help avoid the complicated traditional process design by multiple optimization objectives, the ductile-oriented removal could be the only optimized parameters for both the quality and efficiency.

Based on the above literature review, it could be found that the grinding of brittle materials is a complicated combined process of ductile and brittle removal modes. This paper is devoted to investigate ductility-oriented grinding mechanism and process design for quality and efficiency in high-speed grinding of silicon carbide ceramics. The Rayleigh chip thickness and critical chip thickness models are used to calculate the ductile removal proportion with integral solution. The grinding SEM topography, forces, damages, and specific energy are discussed in detail to reveal the high-speed grinding mechanism. Finally, the process designs for better surface finish and ductility-oriented surface are conducted to achieve a better grinding efficiency with good quality.

2 Rayleigh-based ductile removal calculation

2.1 Chip thickness model

The grinding wheel is always composed of numerous irregular abrasive grits, which will interact with the workpiece material at different chip thicknesses. For the whole grinding wheel, the chip thickness h for a single grit is generally assumed as a stochastic distribution. The Rayleigh chip thickness model is a recognized model, which could be given as [21]:

$$f(h) = \begin{cases} \left(h/\sigma^2\right)e^{h^2/2\sigma^2} & h \geq 0. \\ 0 & h \geq 0 \end{cases} \quad (1)$$

where σ is a parameter that defines the probability function. From Fig. 1, h is the random interacted chip thickness, which varies with different grits and interaction stages. In the above Rayleigh chip thickness model, it will be valid when $\int f(h)dh = 1$. The chip thickness distribution function is depicted in Fig. 2. Then, the expected value $E(h)$ and standard deviation SD(h) could be integrally calculated as:

$$E(h) = \sqrt{\frac{\pi}{2}}\sigma \quad (2)$$

$$SD(h) = \sqrt{0.429\sigma} \quad (3)$$

Then, solving the function parameter σ is crucial for the model setup. It is generally solved by the motion basics such that the removed material volume by the wheel and the lost material volume of the workpiece are equal [20], which could be expressed as:

$$E(A_w)V_S = V_w a_e b_w \quad (4)$$

where A_w is the chip cross-section thickness of all grits, V_s and V_w are the wheel and workpiece rotational linear speeds, b_w is the width of the wheel–workpiece interaction in plunge grinding, and a_e is the depth of cut. Therefore, the whole chip cross-section thickness (A_w) could be calculated as:

$$A_w = A_c.N_d = N_d.h^2.\tan\theta \quad (5)$$

where N_d is the active grits density (numbers in unit area). A_c is the cross section area for a random single grit, which could be calculated by $A_c = h^2 \cdot \tan\theta \cdot \theta$, the semi-included angle of the chip thickness. The active grits density (N_d) can be calculated by static grain density (C_d); it can be expressed as:

$$N_d = C_d.\mathrm{l_g}.b_w \quad (6)$$

$$C_d = 4\chi/\left\{d_g^2(4\pi/3\omega)\rightarrow^{2/3}\right\} \quad (7)$$

where d_g represents the equivalent spherical diameter of the abrasive grain. l_g is the contact arc length. ω and χ are, respectively, the volume fracture of diamond grain and the proportion of diamond grains that are actively engaged in the cutting process. The grinding wheel has a concentration density of 150; thus, the volume fraction ω is 0.375 [22]. Moreover, it is assumed that one-half of the diamond particles are actively engaged in the grinding process [23].

Thus, through the calculation of the expected value of Eq. (4), the function parameter σ could be solved to be:

$$\sigma = \sqrt{\frac{a_e.V_W}{2V_s.C_d}\frac{1}{\mathrm{l_g}.\tan\theta}} \quad (8)$$

Therefore, it could be found that the function parameter is fully defined by the grinding process parameters and wheel specification.

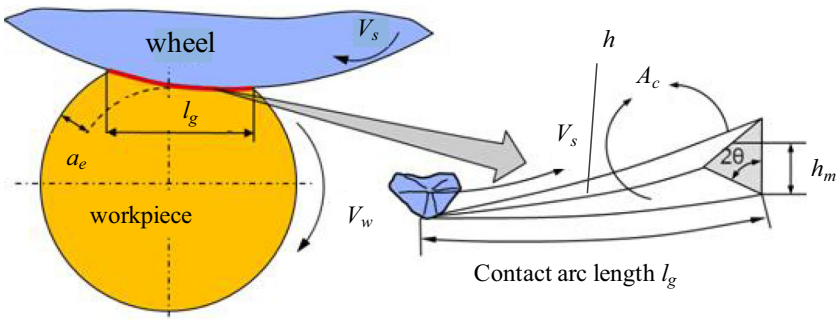

Fig. 1 Theoretical chip thickness

2.2 Ductility-oriented model

Figure 2 is the depicted Rayleigh chip thickness model; the dotted line is the critical chip thickness value. When the theoretical maximum chip thickness (h_m) is smaller than the critical chip thickness, the material will be removed by the ductile mode; otherwise, it would be the brittle mode. The theoretical maximum chip thickness for a single grit in Fig. 1 is given as [24]:

$$h_m = \left(\frac{3}{C_d.\tan\theta}.\frac{V_w}{V_s}.\sqrt{\frac{a_e}{d_e}}\right)^{\frac{1}{2}} \tag{9}$$

where d_e is the equivalent diameter, $d_e = d_s.\, d_w/(d_s + d_w)$ and d_s, and d_w are the diameters of the wheel and workpiece. Based on the material removal energy, Bifano et al. [13] modeled a critical ductile removal value which is independent of the process parameters and only correlated with the materials' mechanical properties. Later on, Chen et al. [25] and Wu et al. [14] modeled a new chip thickness model on the basis of the energy model proposed by Bifano. It was given as [14]:

$$h_{cr} = \beta\left[a + b\ln\left(\frac{V_S}{h_m}\right)\right]^2\left(\frac{E_w}{H_v}\right).\left[\frac{K_{1C}}{H_V}\right]^2 \tag{10}$$

where β is a material constant and it is given as 0.15 [13]. a and b are material constants after considering the dynamic effect brought by process parameters. For SiC, the constants a and b were given as − 1.64 and 0.675 [14]. K_{1C}, E_w, and H_V, respectively, are the fracture toughness, elastic modulus, and hardness of the material.

Thus, the value of Eq. (10) could be depicted as the dotted line in Fig. 2, which is the determination of the ductile or brittle grinding mode. Based on Eqs. (1), (8), and (10), the stochastic percentage for ductile-oriented grinding δ_d could be calculated as:

$$\delta_d = \int_0^{h_{cr}} f(h)dh = 1 - e^{-\frac{h_{cr}^2}{2\sigma^2}} \tag{11}$$

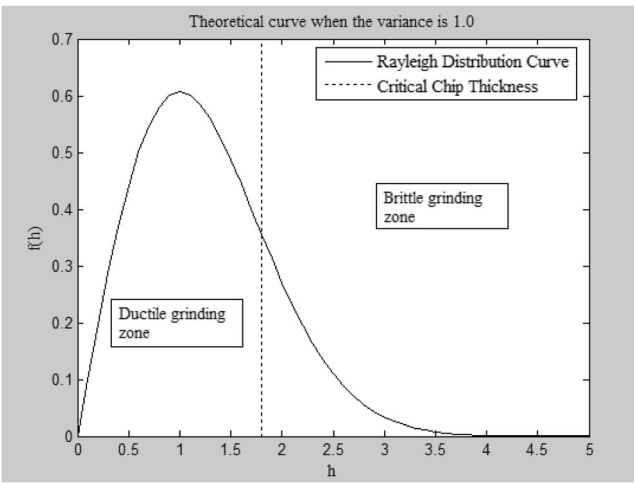

Fig. 2 Rayleigh chip thickness model

3 Experimental setup

The grinding experiments' layout is depicted in Fig. 3. In this work, the grinding tests are conducted on a high-speed cylindrical CNC grinder MGKS1332/H, which could reach a wheel speed of up to 150 m/s. The detailed configuration for the grinding experiments is listed in Table 1. In this paper, a vitrified diamond grinding wheel, with diamond concentration of 150%, diameter 400 mm, and width 22 mm, was used. The wheel was balanced below 0.02 μm with a dynamic balancing instrument (model SB-4500) before grinding tests. A series of plunge grinding experiments are conducted in this paper. The grinding forces are measured by a 3-direction force transducer (Kistler 9347C) mounted in the tailstock which transfers the force signal to a charge amplifier, then to the data acquisition system LMS.

The workpiece is designed as a column sample in Fig. 4a, which has a width of 20 mm and a diameter of 60 mm. The workpiece materials used in this paper are reaction-sintered SiC; the mechanical properties can be found in Table 2. In order to observe the surface and subsurface topographies, the workpiece is divided into two parts in Fig. 4a. From Fig. 4b, it can be seen that the SiC specimen is pasted and polished to the final mirror surface in Fig. 4c. In this paper, the environment scanning electron microscope (ESEM) QUANTA 250 from Czech was used to observe the ground surface and subsurface topographies. The surface roughness is measured by a nanosurface white light interferometer (Bruker Npflex),

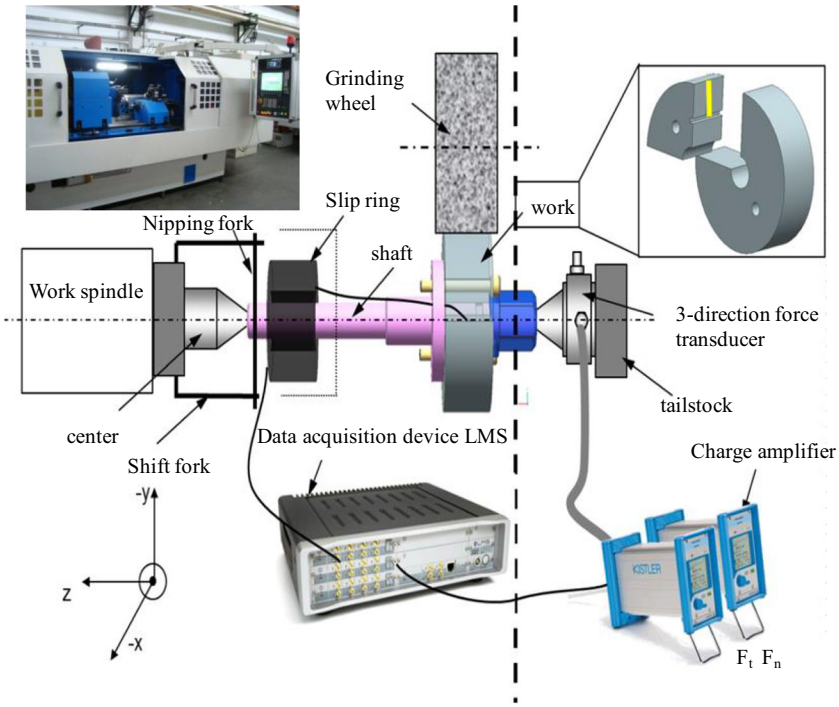

Fig. 3 Experimental layout

which has a sub-nanometer resolution for high-precision measurement of both 2D and 3D surface roughness.

4 Results and Discussions

4.1 Ductility-oriented grinding topography

In order to reveal the effect of process parameters on ductility-oriented percentage (DOP) in Eq. (11) and the related surface topography, Table 3 gives the detailed process parameters and calculated critical chip thickness with Eq. (10). From Table 3, it could be found that when the maximum chip thickness is close to or less than the critical chip thickness, the DOP value is much higher, such as that in test nos. 4 and 7. Thus, the higher percentage for ductile grinding area could happen and more abrasive grits interact and remove material in ductile mode. In Table 3, nos. 1–3 and 4–6 are used to reflect the variation of wheel speed under different chip thicknesses. Nos. 3 and 6–9 are trying to explore the chip thickness effect on grinding surface integrity under a high-grinding speed (140 m/s). Moreover, nos. 10–19 are trying to reflect the effect of process parameters on grinding quality in Figs. 7 and 8.

Figure 5 is the variation of ground surface topography under different process parameters. In this figure, the grinding wheel speed increases from 20 to 140 m/s at different maximum chip thicknesses of 0.52 μm and 1.04 μm. From Fig. 5 (nos. 1, 2, and 3), it could be found that when the DOP increases from 62% at 20 m/s to 65% at 80 m/s and 74% at 140 m/s, the ground surface fracture cracks diminish and more ductile plastic stripes were produced, which means that the increase of wheel speed helps improve the DOP and reduce the surface cracks with more ductile-removed surface. While for the corresponding surface roughness in Fig. 6 (nos. 1, 2, and 3), the surface roughness drops down from 0.457 μm at 20 m/s to 0.187 μm at 140 m/s with a smoother surface. When

Table 1 Experimental conditions

Title	Specification
Wheel	Vitrified Diamond Wheel D91 V+ 2046 J1SC-23 C150 E
Grinding mode	Upgrinding
Wheel speed	20-140 m/s
Workpiece speed	50–1000 mm/s
Depth of cut	2–20 μm
Cooling	Water-based emulsion 5% (10 L/min)
Wheel spindle balancing	SBS Model SB-4500 below 0.02 μm
Workpiece material	SiC

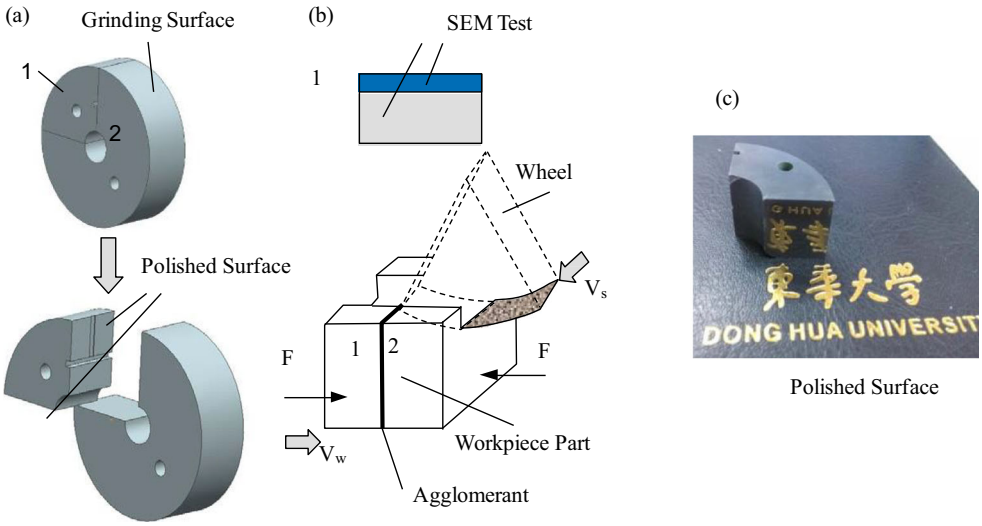

Fig. 4 The workpiece design for SEM tests

the h_m keeps constant at 1.04 μm (Fig. 5 (nos. 4, 5, and 6)), the DOP also increases from 48 to 68% with the increase of wheel speed from 20 to 140 m/s, accompanied by surface roughness (Ra) dropping down from 0.571 to 0.255 μm in Fig. 6 (nos. 4, 5, and 6). In Figs. 5 and 6, it could also be found that the variation of the maximum chip thickness (h_m) could affect the ground surface topography and surface roughness.

Figure 7 shows the effect of wheel speed (V_s), depth of cut (a_e), and workpiece speed (V_w) on the DOP. It could be found that the DOP increases with the increase of wheel speed (V_s), while decreasing with the increase of depth of cut (a_e) and workpiece speed (V_w). This could be explained by Eq. (11), which has a negative correlation with the critical chip thickness (h_{cr}) in Eq. (10). In Fig. 8, the effect of wheel speed (V_s), depth of cut (a_e), and workpiece speed (V_w) on the surface roughness is depicted, which reflects a reverse trend with the DOP. It could be further proved that the increase of DOP could decrease the surface roughness value with more ductile removal.

In Fig. 9, the effect of h_m on the DOP has been given with SEM figures and surface roughness at a constant wheel speed of 140 m/s. From Fig. 9 (nos. 1, 2, 3), it can be seen that the DOP increases from 37% at h_m of 1.8 μm to 91% of 0.31 μm and finally 96% of 0.16 μm, which shows that the reduction of h_m helps substantially improve the surface ductile grinding percentage and more grits remove the material at a ductile mode. Likewise, the surface roughness in Fig. 9 (nos. 4, 5, 6) decreases from 0.615 to 0.165 μm and 0.155 μm. This could be well explained by Eqs. (9) and (11) that the increase of h_m at a constant wheel speed could be caused by an increase of either workpiece speed or depth of cut, which will inevitably bring the increase of material removal rate (Q'_w). Thus, less fracture cracks on the ground surface will be produced with better surface roughness at a lower h_m.

From the above analysis, it can be concluded that the increase of wheel speed or decrease of maximum chip thickness could enhance the percentage to a more ductile-oriented removal mode, which will cause a better surface roughness with fewer fracture cracks and more plastic removal stripes.

4.2 Grinding forces and specific energy

In the grinding process, the grinding force is an important indicator to evaluate the grinding kinetics and removal mechanism. The typical grinding force signal was given in Fig. 10; the right curve is the filtered signal. In order to analyze the grinding force characteristics, a set of 30 different process conditions are given in Table 4. In this table, test nos. 1–12 is the variation of process parameters under a constant material removal rate or speed ratio under multiple factors' variation, while test nos. 13–30 reflect a single wheel speed variation under different depths of cut (a_e) or workpiece speed (V_w).

In Table 4, the specific tangential and normal forces in unit contact length are calculated. In order to analyze the effect of wheel speed (V_s), workpiece speed (V_w), and depth of cut (a_e) on the grinding forces, the multiple linear regression equation is described as:

$$F = m_f \cdot V_S^{x_0} \cdot Vs_w^{y_0} \cdot a_e^{z_0} \tag{12}$$

where m_f is the comprehensive factor, x_0, y_0, and z_0 are the corresponding sensitivity factors. Then through logarithmic calculation and the regression analysis of the equations, the empirical model could be given as:

$$\begin{cases} F'_n = 2.76 \cdot V_s^{-0.33} \cdot V_w^{0.16} \cdot a_e^{0.16} \\ F'_t = 2.36 \cdot V_S^{-0.1} \cdot V_w^{0.09} {}^{0.2}_{e} \end{cases} \tag{13}$$

From the empirical model (Eq. 13), it could be found that both the tangential and normal forces decrease with the increase of the wheel speed and the tangential force decreases slower than the tangential force. However, the increase of

Table 2 Mechanical properties for SiC

Density, ρ_{SiC} (g/cm^3)	Hardness, H_v (GPa)	Fracture toughness, K_{1C} (MPa m$^{1/2}$)	Elastic modulus, E_w (GPa)	Poisson rate, μ_{SiC} (–)
3.05	23	3.0	350	0.16

workpiece speed and depth of cut has a direct ratio with the grinding forces. From the sensitivity factors, the normal force has a close effect with the workpiece speed and depth of cut. While for the tangential force, it is more affected by the depth of cut than workpiece speed.

The specific grinding energy is the consumed energy for unit removal material volume, which is used to indicate the consumed energy and the related removal mode. For brittle materials, the material removal coexists with ductile and brittle modes, which is highly related with the specific grinding energy. The ductile plastic deformation energy is always the dominant grinding energy, which could indicate the change of material removal mode. The specific grinding energy could be calculated as [26]:

$$E = \frac{F_t' \cdot V_S}{Q'_w} = \frac{F_t' \cdot V_S}{a_e \cdot V_w} \tag{14}$$

where Q'_w is the material removal rate (mm^3/(mm s)); it is generally given as:

$$Q'_w = a_e \cdot V_w \tag{15}$$

Figure 11 reflects the variation of specific energy under different process parameters. It can be found from Fig. 9a that when the material removal rate (Q'_w) is kept constant, the increase of wheel speed (V_s) causes an increase of specific energy. From Eqs. (13) and (14), although the increase of wheel speed could reduce the specific tangential force F_t', the increase of wheel speed is much higher than the decrease of F_t'. Moreover, from section 4.1, the increase of wheel speed could help increase the ductile-oriented grinding, which will enhance the plastic deformation energy and thus increase the specific grinding energy E.

Figure 11b, c, and d show the increases of workpiece speed (V_w), depth of cut (a_e), and maximum chip thickness (h_m) will lead to a reduction of specific grinding energy at a constant wheel speed of 140 m/s. This could be well understood from Eq. (14) that the material removal rate (Q'_w) substantially increases with the increase of workpiece speed (V_w) and depth

Table 3 Process parameters for high-speed ductile-oriented percentage (DOP)

No.	Wheel speed, V_s (m/s)	Workpiece speed, V_w (mm/s)	Depth of cut, a_e (μm)	Maximum chip thickness, h_m (μm)	Critical chip thickness, h_{cr} (μm)	Ductile-oriented percentage (DOP) δ_d (%)
1	20	25	3	0.52	0.04	62
2	80	100	3	0.52	0.16	65
3	140	100	9.2	0.52	0.24	74
4	20	75	5.2	1.04	0.007	48
5	80	300	5.2	1.04	0.09	54
6	140	300	15.9	1.04	0.15	68
7	140	16	3	0.16	0.47	96
8	140	100	1	0.31	0.32	91
9	140	900	15.9	1.8	0.09	37
10	20	100	8	1.34	0.18	25
11	60	100	8	1.05	0.39	32
12	100	100	8	0.82	0.55	71
13	140	100	8	0.69	0.68	89
14	100	100	5	0.73	0.58	81
15	100	100	12	0.90	0.53	61
16	100	100	16	0.97	0.52	54
17	100	160	5	0.92	0.53	6
18	100	240	5	1.12	0.48	40
19	100	300	5	1.25	0.46	32

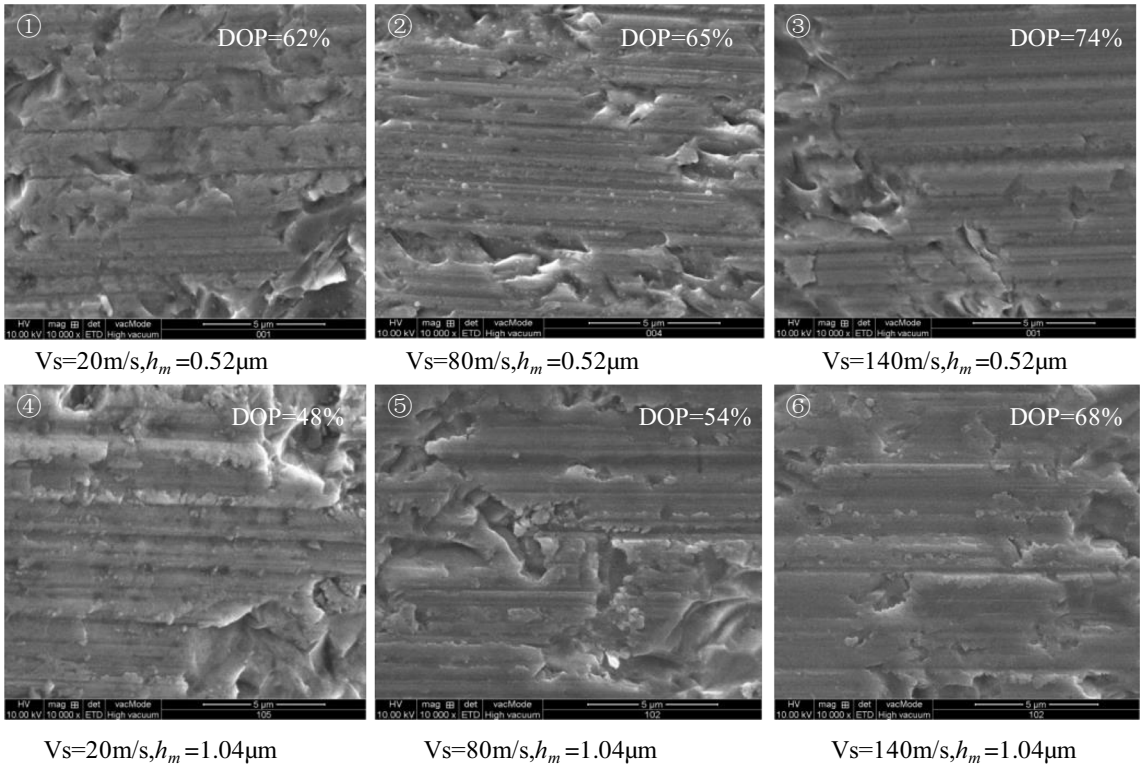

Fig. 5 SEM topography under different wheel speeds and maximum chip thicknesses

of cut (a_e), while the grinding forces just slightly enhance from Eq. (13). Moreover, the maximum chip thickness (h_m) in Eq. (9), respectively, has quadratic and quartic relations with V_w and a_e, which could lead to a much higher Q'_w elevation with the increase of h_m. Thus, the increase of h_m could cause a higher reduction of the specific grinding energy, from 455 J/mm^3 at h_m of 0.16 μm to 31 J/mm^3 at h_m of 1.8 μm, compared with the Q'_w increment from 0.047 to 14.3 mm^3/(mms).

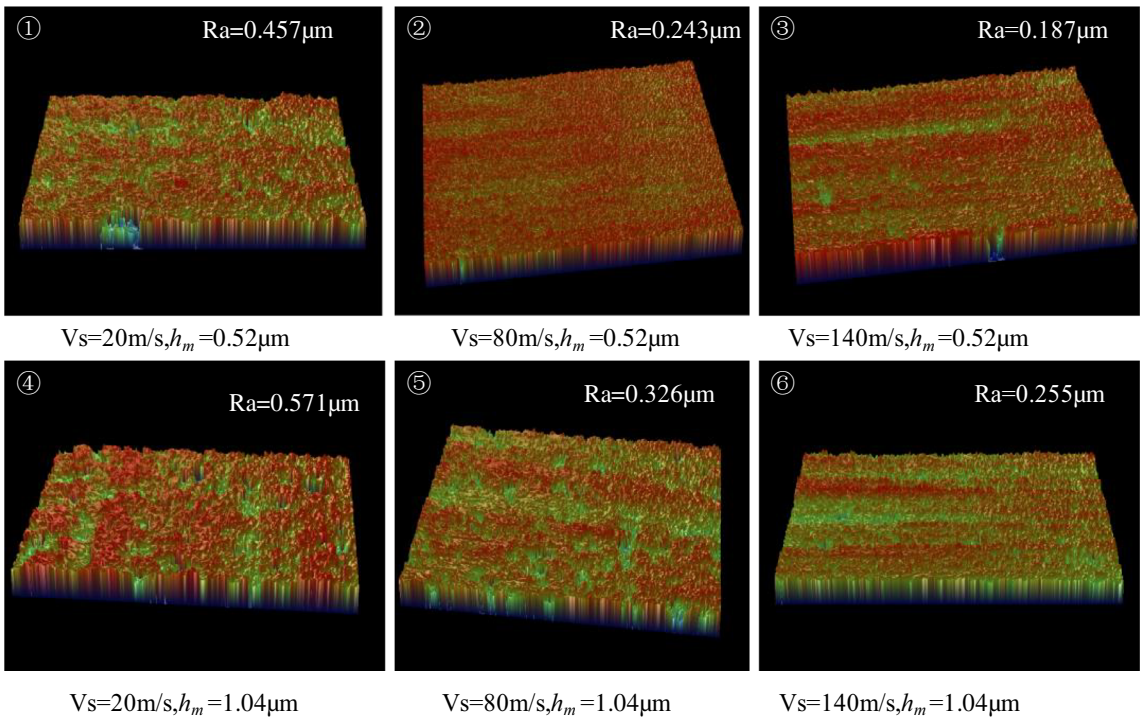

Fig. 6 3D surface roughness under different wheel speeds and maximum chip thicknesses

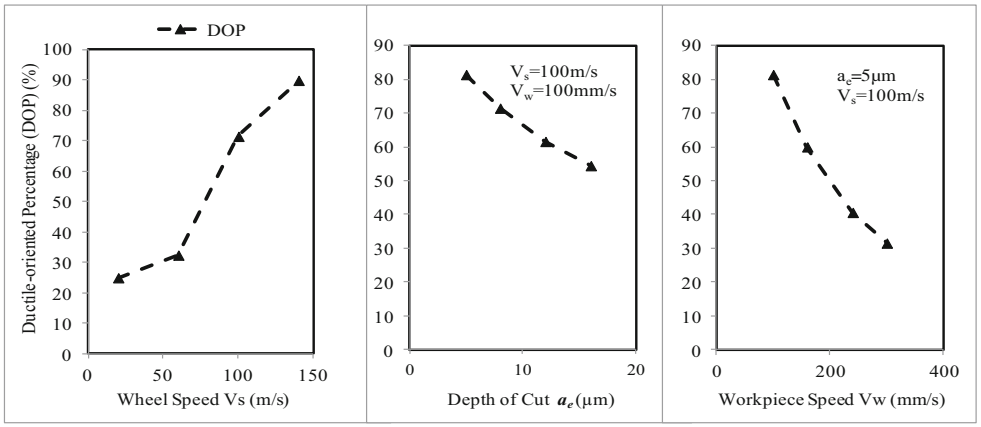

Fig. 7 DOP variation under different process parameters

From Eqs. (9) and (13) and Fig. 11, it can also be found that the increase of workpiece speed (V_w) could better help to reduce grinding force and facilitate the ductile removal at a higher specific grinding energy with higher Q'_w than the increase of depth of cut (a_e).

4.3 Grinding damage control with efficiency

Grinding damages are the key factors that affect ceramics grinding quality and efficiency. There are generally two kinds of damages that could be induced in the grinding process: Surface damage (SD) is produced by lateral cracks and subsurface damage (SSD) by median cracks [20]. In order to quantitatively analyze the grinding damages, the surface and subsurface damage crack sizes are measured as Fig. 12. In Fig. 12, the surface crack size is determined by the average size of the five largest crack sizes, while the subsurface size is measured by the general depth size. From Fig. 12, it can be found that the variation of wheel speed V_s and maximum chip thickness (h_m) could affect the grinding damages and h_m has a more intense impact on the grinding damages than the wheel speed (V_s).

By considering the grinding process, the grinding damages are always be modeled as [27]:

$$\begin{aligned} C_l &= 0.43(\sin\theta)^{1/2}(\cot\theta)^{1/3}(E_W/H_V)^m(P/H_V)^{1/2} \\ C_m &= {\alpha_k}^{2/3}(E_W/H_V)^{(1-m)2/3}(\cot\theta)^{4/9}(P/K_{1C})^{2/3} \end{aligned} \tag{16}$$

where C_l and C_m are the lateral and median crack lengths, which could be related to SD and SSD. m and α_k are the model coefficients. In this model, the indentation load P is highly related to the grinding force in Eq. (13) [27, 28]. From Eqs. (9) and (13), it could be found that the effect of process parameters on grinding damages could be highly reflected on the variation of V_s and h_m.

Figure 13 shows the wheel speed effect on the grinding forces and damages. From Fig. 13a, it could be found that the tangential force is kept stable at a low rangeability with a reduction of surface crack size when the wheel speed increases from 20 to 140 m/s, while the material removal rate (Q'_w) increases from 0.075 to 0.525 $mm^3/(mms)$. Similar results could be found in Fig. 13b with normal force and subsurface crack size variations. In Fig. 13b, when the wheel speed increases from 20 to 140 m/s, the normal force increases 10% with increase of material removal rate (Q'_w) from 0.075

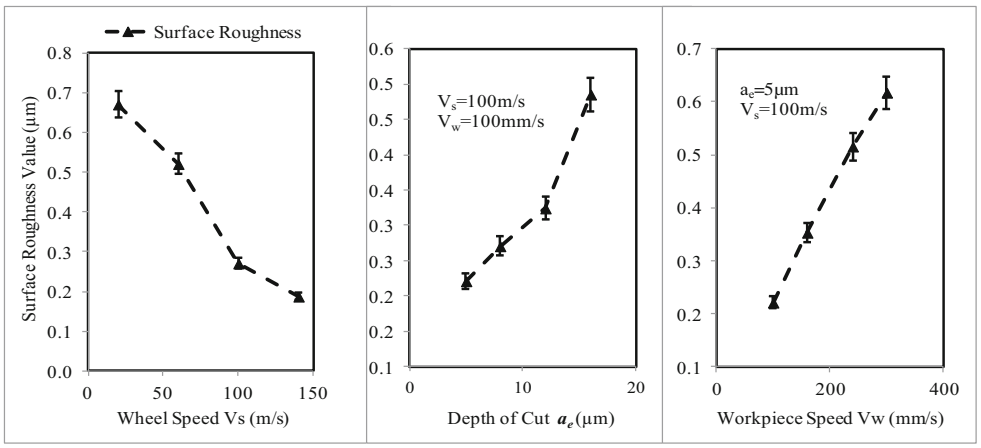

Fig. 8 Surface roughness value variation under different process parameters

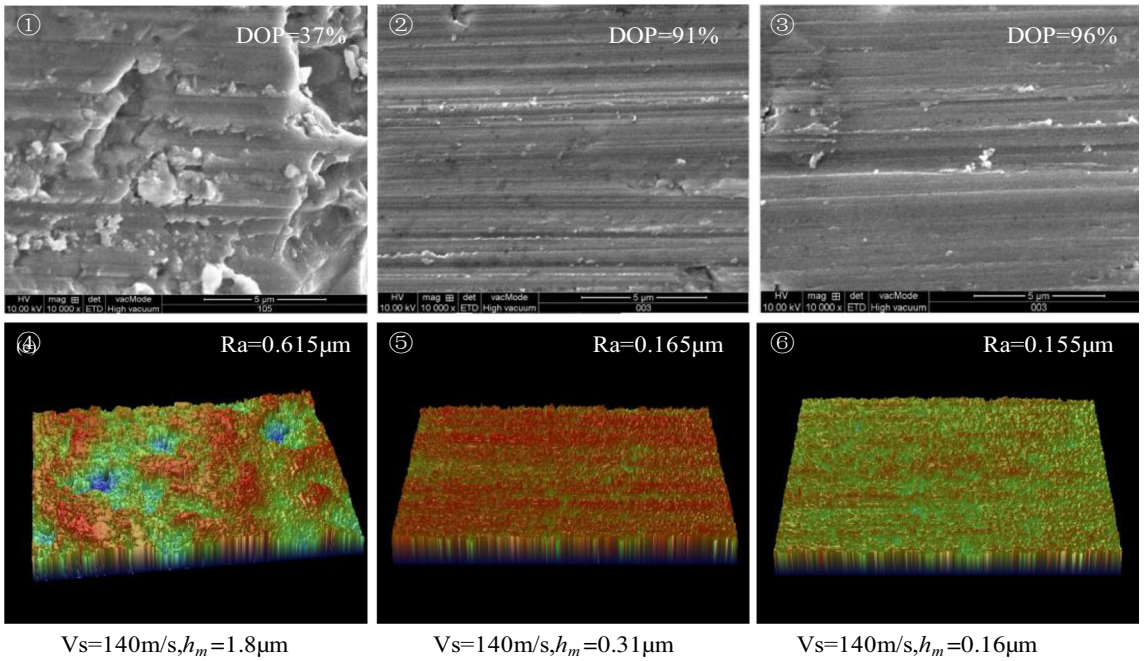

Fig. 9 Surface topography and roughness under different maximum chip thicknesses

to 0.525 mm^3/(mms), while the subsurface crack size drops 50%. Therefore, it could be found that the increase of wheel speed could help reduce the grinding damages at a relative high material removal rate and stable grinding forces.

Figure 14 is the maximum chip thickness h_m effect on grinding forces and damages at a wheel speed of 140 m/s. In this figure, the maximum chip thickness h_m increases from 0.31 to 1.04 μm, and the material removal rate (Q'_w) increases from 0.1 to 2.73 mm^3/(mms). From Fig. 14a and b, it could be found that the increases of maximum chip thickness (h_m) could cause a sharp increase of grinding forces and crack size. The value of the grinding forces and crack size at h_m of 1.04 μm is 6–10 times of 0.31 μm, compared with the increase of about 27 times of Q'_w increase. That is to say, although the increase of maximum chip thickness h_m will inevitably deteriorate the grinding quality and increase grinding forces, the grinding efficiency could be improved with higher Q'_w. Therefore, under the premise of the quality requirements, a moderate increase of maximum chip thickness h_m with a higher grinding speed could be beneficial for a higher material removal rate, which could be fully explained from model (16).

4.4 Process design for surface roughness and ductile removal

In the grinding process, quality and efficiency are the main requirements for the process design. In this section, the high-speed grinding process for surface roughness below 0.2 μm

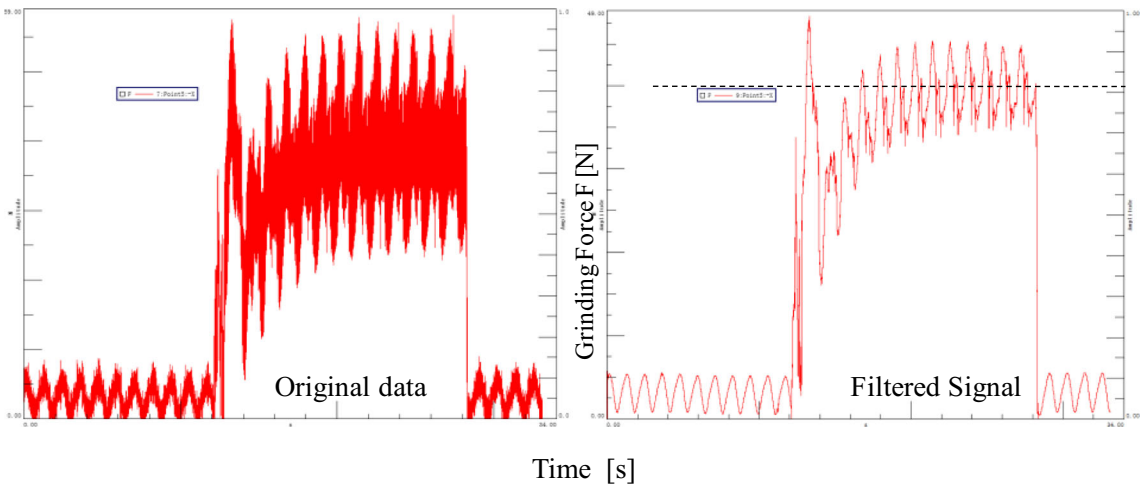

Fig. 10 Force signal and filtered curve

Table 4 Process parameters for grinding force analysis

No.	Wheel speed, V_s (m/s)	Workpiece speed, V_w (mm/s)	Depth of cut, a_e (μm)	Specific normal force, F'_n (N/mm)	Specific tangential force, F'_t (N/mm)
1	80	400	2.5	2.67	1.07
2	80	600	1.7	2.33	0.80
3	80	800	1.3	2.22	0.60
4	80	1000	1.0	1.87	0.40
5	20	67	15.0	2.18	1.20
6	40	133	7.5	1.42	0.54
7	60	200	5.0	1.12	0.27
8	80	267	3.8	0.85	0.13
9	20	80	17.0	2.22	0.66
10	40	160	17.0	2.38	1.01
11	60	240	17.0	2.59	1.27
12	80	320	17.0	2.67	1.50
13	20	100	5.0	3.14	1.09
14	40	100	5.0	2.52	0.82
15	60	100	5.0	2.05	0.61
16	80	100	5.0	1.57	0.47
17	100	100	5.0	1.30	0.39
18	120	100	5.0	1.02	0.34
19	20	200	5.0	3.55	1.57
20	40	200	5.0	2.93	1.16
21	60	200	5.0	2.59	0.95
22	80	200	5.0	1.98	0.89
23	100	200	5.0	1.70	0.75
24	120	200	5.0	1.43	0.67
25	20	100	10.0	4.57	1.77
26	40	100	10.0	3.95	1.50
27	60	100	10.0	3.27	1.23
28	80	100	10.0	2.73	1.22
29	100	100	10.0	2.59	1.17
30	120	100	10.0	2.32	1.09

and ductility-oriented grinding for more than 50% DOP are designed for a better surface finish and efficiency in the semi-precision grinding process. In this part, the grinding experiments for wheel, machine tools, and workpiece are given in

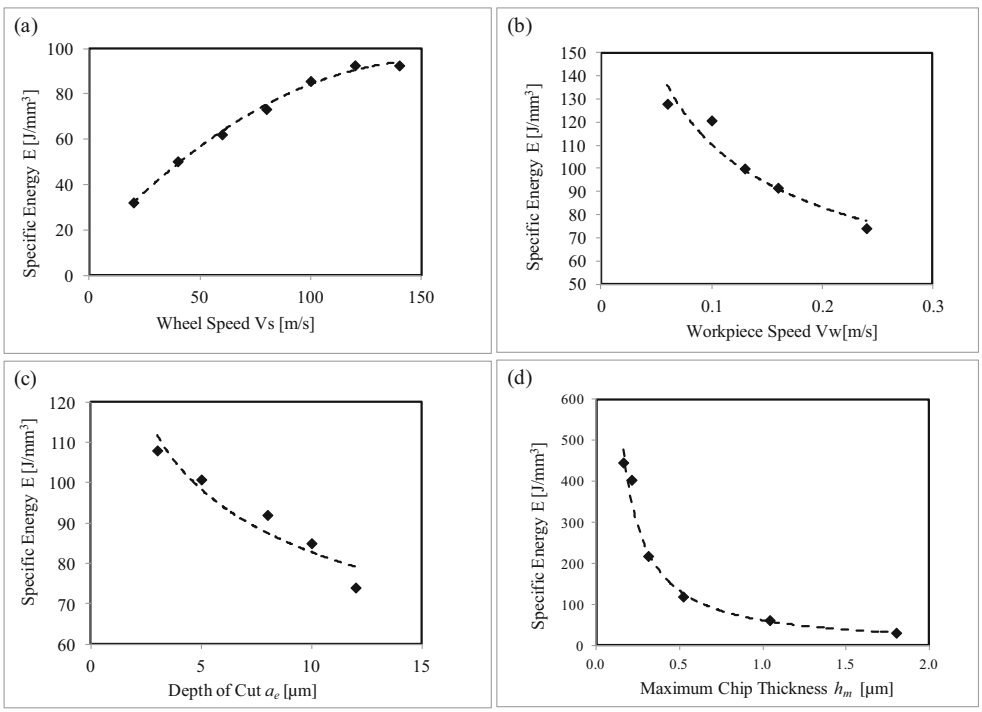

Fig. 11 The variation of specific energy under different process parameters

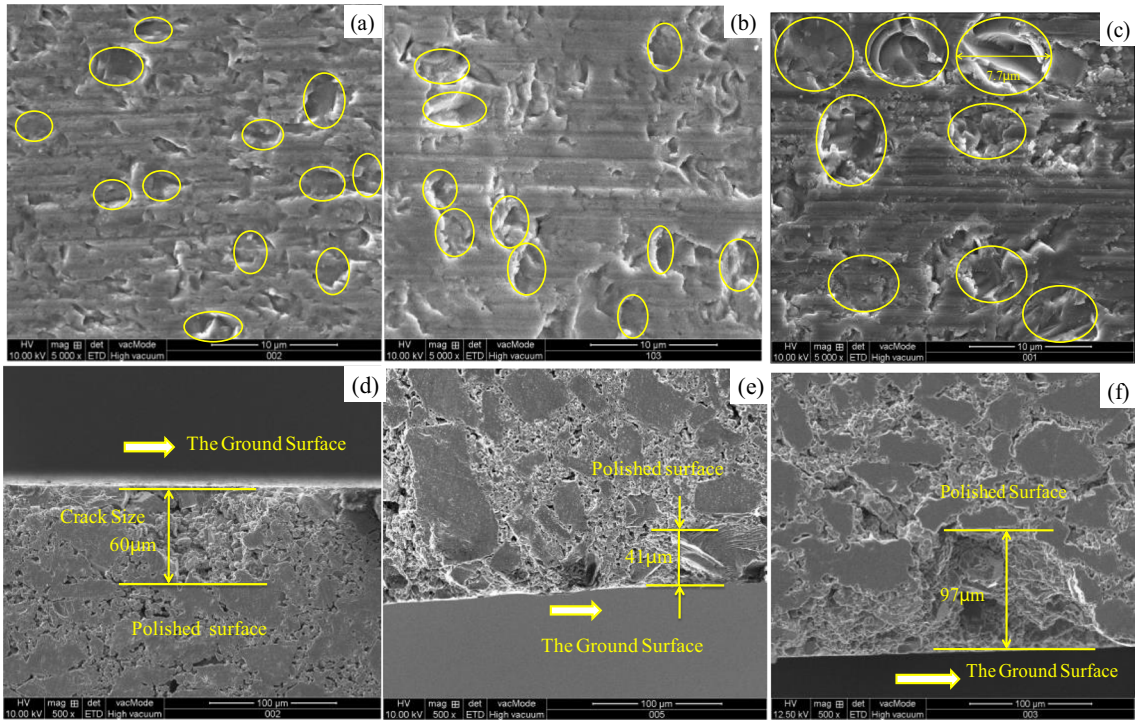

Fig. 12 Surface/subsurface damage SEM topology for SiC at V_s = 80 m/s, h_m = 0.52 μm (**a**, **d**); V_s = 140 m/s, h_m = 0.52 μm (**b**, **e**); V_s = 140 m/s, h_m = 1.04 μm (**c**, **f**); × 5000 (**a**, **b**, **c**); × 500 (**d**, **e**, **f**)

Fig. 13 Wheel speed effect on grinding forces and damages

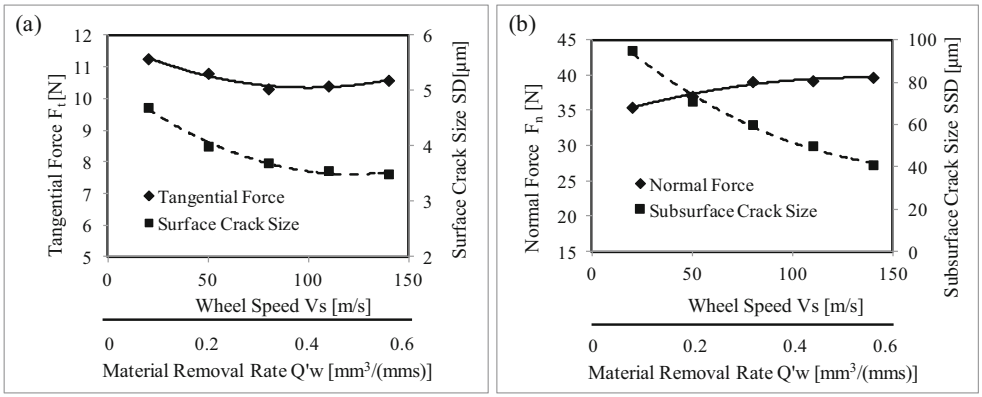

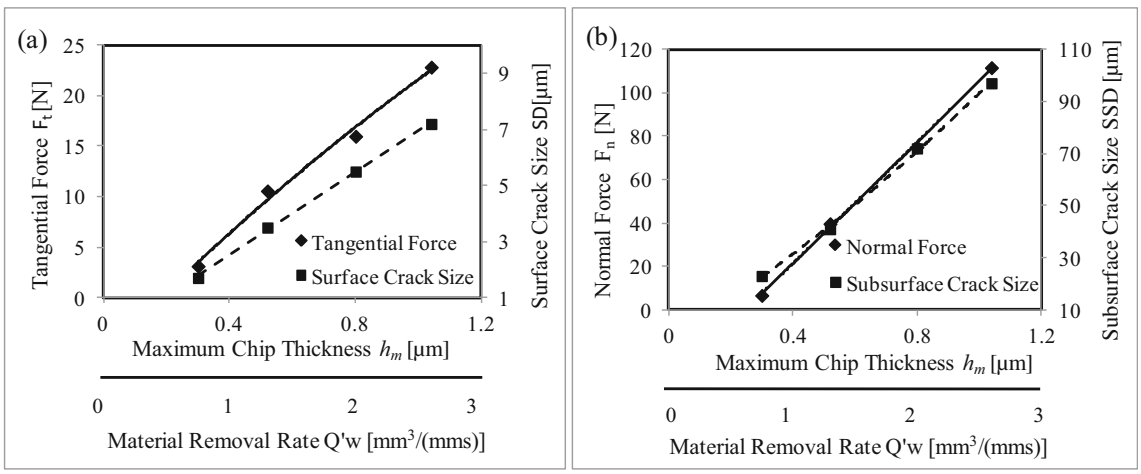

Fig. 14 Maximum chip thickness (h_m) effect on grinding forces and damages

Table 5 Optimization target

Optimization target	Data
Surface roughness	Ra ≤ 0.2 μm
DOP	Higher than 50%

Table 1. Table 5 is the optimization target for the precision grinding of silicon carbide ceramics.

Figure 15 shows the process suggestion for a surface roughness below Ra 0.2 μm. Figure 15a and b respectively give the effect of wheel speed and chip thickness on ground surface roughness Ra and ductility-oriented removal percentage DOP. For Fig. 15a at a constant maximum chip thickness (h_m), it could be found that the increase of wheel speed could help reduce the surface roughness value with a higher DOP. In the meanwhile, the material removal rate (Q'_w) increases from 0.075 to 0.525 mm^3/(mms). In Fig. 15b, the increase of maximum chip thickness (h_m) shows an opposite result compared with the wheel speed increase, leading a huge increase of the material removal rate (Q'_w) from 0.1 to 2.73 mm^3/(mms).

In Fig. 15a, for the surface roughness process target under 0.2 μm, the color column shows the process region of the wheel speed higher than 137 m/s with a minimum material removal rate (Q'_w) 0.55 mm^3/(mms) and 87% DOP. While for Fig. 15b, the process region for 0.2 μm surface roughness target, it is suggested to conduct under a maximum chip thickness h_m of 0.56 μm with a maximum material removal rate (Q'_w) of 1.1 mm^3/(mms) and minimum 83% DOP. Under these circumstances, the ductile grinding could be achieved with minimum 83% DOP, which shows a dominant ductile-oriented removal process.

Therefore, for surface roughness value under 0.2 μm, it is suggested to conduct the grinding process at a wheel speed (V_s) higher than 137 m/s and maximum chip thickness (h_m) below 0.56 μm, which could help achieve a material removal rate between 0.55 and 1.1 mm^3/(mms) with minimum 83% DOP.

Figure 16 shows the ductility-oriented grinding process for a DOP higher than 50%. It could be found from Fig. 16a that when the grinding wheel speed is higher than 53 m/s, the ductile grinding region DOP could be higher than 50% and the surface roughness value will remain below 0.325 μm with

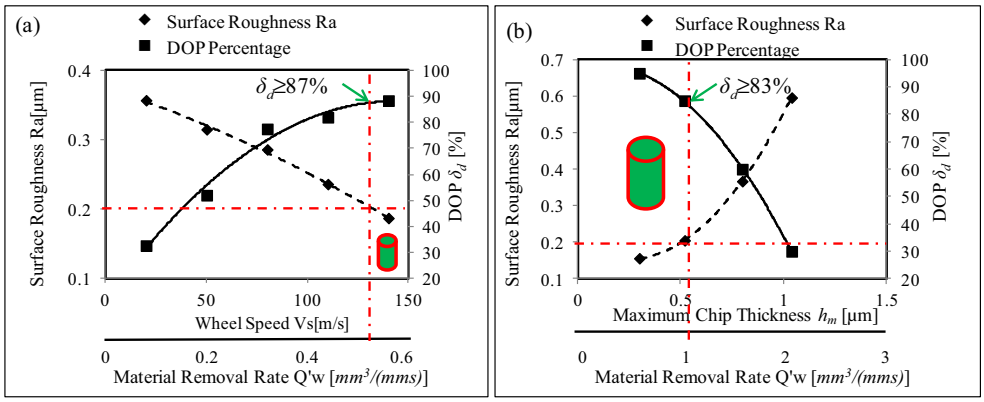

Fig. 15 Surface roughness target for process optimization with efficiency

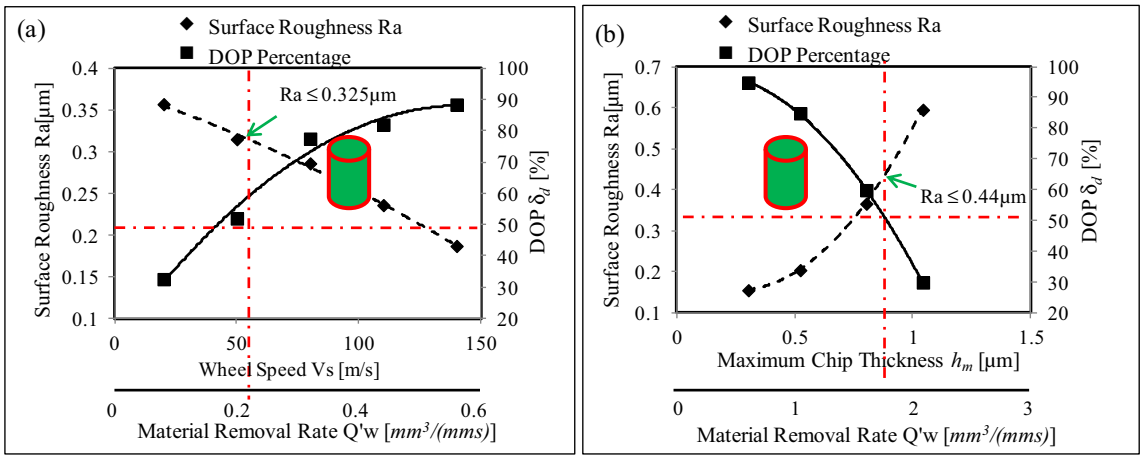

Fig. 16 Ductility-oriented process optimization for efficiency

a minimum material removal rate (Q'_w) 0.2 mm^3/(mms). From Fig. 16b, when the maximum chip thickness (h_m) is lower than 0.78 μm, the maximum material removal rate (Q'_w) could reach up to 1.5 mm^3/(mms) with a maximum surface roughness value of 0.44 μm.

Thus, for DOP higher than 50%, it is suggested to conduct the grinding process at a wheel speed (V_s) higher than 53 m/s and maximum chip thickness (h_m) below 0.78 μm. Under this process condition, the material removal rate (Q'_w) could be varied between 0.2 and 1.5 mm^3/(mms) with a maximum surface roughness of 0.44 μm.

5 Conclusions

In this paper, the ductile-oriented grinding mechanism and process design are investigated to promote grinding quality with a higher efficiency in high-speed grinding of silicon carbide ceramics. The Rayleigh chip thickness model and critical chip thickness model are given to quantitatively calculate the ductile removal proportion, which fully considers the effect of the grinding process condition. Through the grinding experiments and analysis, the following conclusions could be drawn:

1. From the SEM analysis, it can be found that the increase of wheel speed or decrease of maximum chip thickness will be more helpful for higher ductile-oriented removal with smaller surface roughness value, fewer fracture cracks, and more plastic removal stripes.
2. From the empirical force model, the grinding forces decrease with the increase of the wheel speed, while the increase of workpiece speed and depth of cut has a direct ratio with the grinding forces. From the sensitivity factors, the normal force has a close effect with the workpiece speed and depth of cut. The tangential force is more affected by the depth of cut than the workpiece speed.
3. Although the increase of maximum chip thickness (h_m) will inevitably deteriorate the grinding quality and increase grinding forces, moderate increase of maximum chip thickness (h_m) at a higher grinding speed could be beneficial for higher material removal rate (Q'_w).
4. For surface roughness value under 0.2 μm, it is suggested to conduct the grinding process at a wheel speed (V_s) higher than 137 m/s and maximum chip thickness (h_m) below 0.56 μm, which could help to achieve a material removal rate between 0.55 and to 1.1 mm^3/(mms) with minimum 83% DOP. While for DOP higher than 50%, it is suggested to conducted the grinding process at a wheel speed (V_s) higher than 53 m/s and maximum chip thickness (h_m) below 0.78 μm, which could achieve a material removal rate (Q'_w) between 0.2 and 1.5 mm^3/(mms) with a maximum surface roughness of 0.44 μm.

Funding information This work is supported in by the Fundamental Research Funds for the Shanghai Sailing Program (19YF1401400), the Shanghai Scientific Research Program (17DZ2281000), the Central Universities (2232018D3-14), and China Postdoctoral Science Foundation (2018M630384).

References

1. Agarwal S, Rao PV (2011) Improvement in productivity in SiC grinding. Proc Inst Mech Eng B-J Mech Eng Sci. 225(6):811–830
2. Xiao GB, To S, Zhang GQ (2015) The mechanism for ductile deformation in ductile regime machining of 6H SiC. Comp Mater Sci. 98:178–188
3. Zhu DH, Yan SJ, Li BZ (2014) Single-grit modeling and simulation of crack initiation and propagation in SiC grinding using maximum undeformed chip thickness. Comp Mater Sci. 92:13–21
4. Frangulyan TS, Vasilev IP, Ghyngazov SA (2018) Effect of grinding and subsequent thermal annealing on phase composition of subsurface layers of zirconia ceramics. Ceram Int. 44(2):2501–2503
5. Esmaeilzare A, Rahimi A, Rezaei SM (2014) Investigation of subsurface damages and surface roughness in grinding process of Zerodur® glass–ceramic. Appl Surf Sci. 313:67–75
6. Yue CX, Gao HN, Liu XL, Liang SY, Wang LH (2019) A review of chatter vibration research in milling. Chinese J Aeronaut. 32(2):215–242
7. Huang H, Liu YC (2003) Experimental investigations of machining characteristics and removal mechanisms of advanced ceramics in high speed deep grinding. Int J Mach Tool Manuf. 43(8):811–823
8. Ding ZS, Sun GX, Jiang XH, Guo MX, Liang SY (2019) Predictive modeling of microgrinding force incorporating phase transformation effects. J Manuf Sci Eng Trans ASME. 141(8):081009
9. Jiang XH, Kong XJ, Zhang ZY, Wu ZP, Ding ZS, Guo MX (2020) Modeling the effects of Undeformed Chip Volume (UCV) on residual stresses during the milling of curved thin-walled parts. Int J Mech Sci. 167:105162. https://doi.org/10.1016/j.ijmecsci.2019.105162
10. Wu CJ, Pang JZ, Li BZ, Liang SY (2019) High-speed grinding of HIP-SiC ceramics on transformation of microscopic features. Int J Adv Manuf Technol. 102:1913–1921. https://doi.org/10.1007/s00170-018-03226-4
11. Wang CC, Chen JB, Fang QH, Liu F, Liu YW (2016) Study on brittle material removal in the grinding process utilizing theoretical analysis and numerical simulation. Int J Adv Manuf Technol. 87:2603–2614
12. Yang M, Li CH, Zhang YB, Jia DZ, Zhang XP, Hou YL, Li RZ, Wang J (2017) Maximum undeformed equivalent chip thickness for ductile-brittle transition of zirconia ceramics under different lubrication conditions. Int J Mach Tool Manuf. 122:55–65
13. Bifano TG, Dow TA, Scattergood RO (1991) Ductile-regime grinding: a new technology for machining brittle materials. J Eng Ind Trans ASME. 113(2):184–189
14. Wu CJ, Li BZ, Liang SY (2016) A critical energy model for brittle-ductile transition in grinding considering wheel speed and chip thickness effects. Proc Inst Mech Eng B-J Mech Eng Sci. 230(8):1372–1380
15. Venkatachalam S, Li XP, Liang SY (2009) Predictive modeling of transition undeformed chip thickness in ductile-regime micro-machining of single crystal brittle materials. J Mater Process Technol. 209(7):3306–3319
16. Wang CC, Fang QH, Chen JB, Liu YW, Jin T (2016) Subsurface damage in high-speed grinding of brittle materials considering kinematic characteristics of the grinding process. Int J Adv Manuf Technol. 83:937–948

17. Li HN, Yu TB, Wang ZX, Zhu LD, Wang WS (2017) Detailed modeling of cutting forces in grinding process considering variable stages of grain-workpiece micro interactions. Int J Mech Sci. 126: 319–339
18. Hecker RL, Liang SY, Wu XJ, Jing D (2007) Grinding force and power modeling based on chip thickness analysis. Int J Adv Manuf Technol. 33:449–459
19. Pang JZ, Wu CJ, Shen YM, Liu SQ, Wang QX, Li BZ (2019) Heat flux distribution and temperature prediction model for dry and wet cylindrical plunge grinding. Proc Inst Mech Eng B-J Mech Eng Sci. 233(10):2047–2060
20. Wu CJ, Li BZ, Liu Y, Liang SY (2017) Surface roughness modeling for grinding of silicon carbide ceramics considering co-existing of brittleness and ductility. Int J Mech Sci. 133:167–177
21. Wu CJ, Li BZ, Yang JG, Liang SY (2016) Prediction of grinding force for brittle materials considering co-existing of ductility and brittleness. Int J Adv Manuf Technol 87:1967–1975
22. Malkin S, Hwang TW (1996) Grinding mechanisms for ceramics. CIRP Ann Manuf Technol. 456(2):569–580
23. Agarwal S, Rao PV (2013) Predictive modeling of force and power based on a new analytical undeformed chip thickness model in ceramic grinding. Int J Mach Tool Manuf. 65(2):68–78
24. Simanchal KPP, Bandyopadhyay SP (2017) High speed and precision grinding of plasma sprayed oxide ceramic coatings. Ceram Int. 43:15316–15331
25. Chen MJ, Zhao QL, Dong S (2005) The critical conditions of brittle–ductile transition and the factors influencing the surface quality of brittle materials in ultra-precision grinding. J Mater Process Technol. 168(1):75–82
26. Dai C.W., Yin Z., Ding W.F., Zhu Y.J. (2019) Grinding force and energy modeling of textured monolayer CBN wheels considering undeformed chip thickness nonuniformity. Int J Mech Sci. (157-158):221-230.
27. Lin XH, Ke XL, Ye H, Hu CL, Guo YB (2017) Investigation of surface/subsurface integrity and grinding force in grinding of BK7 glass. Proc Inst Mech Eng B-J Mech Eng Sci. 231(12):2349–2356
28. Shao YM, Li BZ, Liang SY (2015) Predictive modeling of surface roughness in grinding of ceramics. Mach Sci Technol. 19(2):325–338